

# An Experimental Prototype for Multistatic Asynchronous ISAC

Marco Canil  
marco.canil@phd.unipd.it  
University of Padova  
Padova, Italy

Jacopo Pegoraro  
jacopo.pegoraro@unipd.it  
University of Padova  
Padova, Italy

Jesus O. Lacruz  
jesusomar.lacruz@imdea.org  
IMDEA Networks  
Madrid, Spain

Marco Mezzavilla  
mezzavilla@nyu.edu  
New York University  
New York, United States

Michele Rossi  
michele.rossi@unipd.it  
University of Padova  
Padova, Italy

Joerg Widmer  
joerg.widmer@imdea.org  
IMDEA Networks  
Madrid, Spain

Sundeep Rangan  
srangan@nyu.edu  
New York University  
New York, United States

## ABSTRACT

We prototype and validate a *multistatic* millimeter-wave (mmWave) Integrated Sensing And Communication (ISAC) system based on IEEE 802.11ay. Compensation of the clock asynchrony between each transmitter (TX) and receiver (RX) pair is performed using the sole line-of-sight (LoS) wireless signal propagation. As a result, our system provides concurrent target tracking and micro-Doppler ( $\mu$ D) estimation from multiple points of view, paving the way for practical multistatic data fusion. Our results on human movement sensing, complemented with precise, quantitative ground-truth (GT) data, demonstrate the enhanced sensing capabilities of multistatic ISAC, due to the spatial diversity of the receiver nodes.

## KEYWORDS

Integrated Sensing and Communication, Millimeter-wave Sensing, Human Sensing, Multistatic Radar, micro-Doppler, IEEE802.11ay

### ACM Reference Format:

Marco Canil, Jacopo Pegoraro, Jesus O. Lacruz, Marco Mezzavilla, Michele Rossi, Joerg Widmer, and Sundeep Rangan. 2023. An Experimental Prototype for Multistatic Asynchronous ISAC. In *Proceedings of First ACM Workshop on mmWave Sensing Systems and Applications (mmWaveSys)*. ACM, New York, NY, USA, 2 pages. <https://doi.org/XXXXXXX.XXXXXXX>

## 1 INTRODUCTION

Integrated Sensing And Communication (ISAC) reuses wireless network devices for sensing the surroundings by applying the radar principles to communication signals. The strength of this approach lies in the ubiquity of wireless communication devices which avoids the costly deployment of dedicated sensors and allows exploiting spatial diversity and boost sensing accuracy thanks to *multistatic* settings [1]. However, communication devices are based on separated TX and RX nodes with *asynchronous* local oscillators (LOs), which make conventional radar techniques unusable [4]. Several methods exist to mitigate the impact of such asynchrony [4], but none have been experimentally validated on multistatic scenarios.

Permission to make digital or hard copies of all or part of this work for personal or classroom use is granted without fee provided that copies are not made or distributed for profit or commercial advantage and that copies bear this notice and the full citation on the first page. Copyrights for components of this work owned by others than ACM must be honored. Abstracting with credit is permitted. To copy otherwise, or republish, to post on servers or to redistribute to lists, requires prior specific permission and/or a fee. Request permissions from [permissions.acm.org](https://permissions.acm.org).

*mmWaveSys*, November 12, 2023, Istanbul, Türkiye

© 2023 Association for Computing Machinery.  
ACM ISBN 978-1-4503-XXXX-X/18/06...\$15.00  
<https://doi.org/XXXXXXX.XXXXXXX>

We fill this gap by presenting the first experimental prototype of *asynchronous and multistatic* ISAC in the mmWave frequency band, based on the IEEE 802.11ay standard at 60 GHz. The LO asynchrony is compensated for by exploiting the LoS propagation of the signal between each TX and RX pair. Our results on human movement sensing show that the system can accurately track people and estimate their  $\mu$ D signature from multiple points of view, providing enriched and more reliable movement features for advanced sensing applications (e.g., activity recognition). Finally, our measurements are supplemented with marker-based motion tracking GT data, providing, for the first time, a reliable reference to assess both  $\mu$ D and tracking traces.

## 2 SYSTEM OVERVIEW

The system is composed of one TX and two RX antenna arrays exchanging standard-compliant single-carrier IEEE 802.11ay data packets. Every packet includes 12 beam-training fields, each transmitted using a different antenna beam pattern (BP),  $b$ , that are used to estimate the channel impulse response (CIR). The CIR estimates are processed to remove the timing offset (TO) and the carrier frequency offset (CFO) caused by the clocks asynchrony and are used to track the movement of a subject and to extract its  $\mu$ D signature.

### 2.1 Channel Model

At a specific time  $k$ , the estimated CIR is represented as a vector of  $L$  complex channel gains, called *taps*, and indexed by  $\ell$ . Each tap corresponds to a specific propagation delay (and, therefore, path length) of the transmitted signal. Indicating with  $T$  the time between two consecutive channel estimations, with  $N_\ell(kT)$  the number of reflections corresponding to tap  $\ell$ , and with  $A_n(kT)$  the complex signal attenuation coefficient, the CIR is expressed as  $h(k, \ell) = \sum_{n=1}^{N_\ell(kT)} A_n(kT) e^{j2\pi[f_{D,n}(kT) + f_{\text{off}}(kT)]kT}$ , where  $f_{D,n}(\cdot)$  and  $f_{\text{off}}(\cdot)$  represent, respectively, the Doppler frequency induced by targets motion in path  $n$  and the CFO. Since training fields are transmitted with different BPs, corresponding to different directions, each of them yields a different CIR, denoted by  $h_b(k, \ell)$ .

### 2.2 Target tracking and $\mu$ D extraction

**TO compensation.** As explained in [3], it is fundamental to compensate for the TO in order to correctly localize a target. In this work, we assume that a LoS path between TX and RX is available and we use it as a common reference to align the CIR estimates in time. For that, according to a dynamic threshold, we detect the

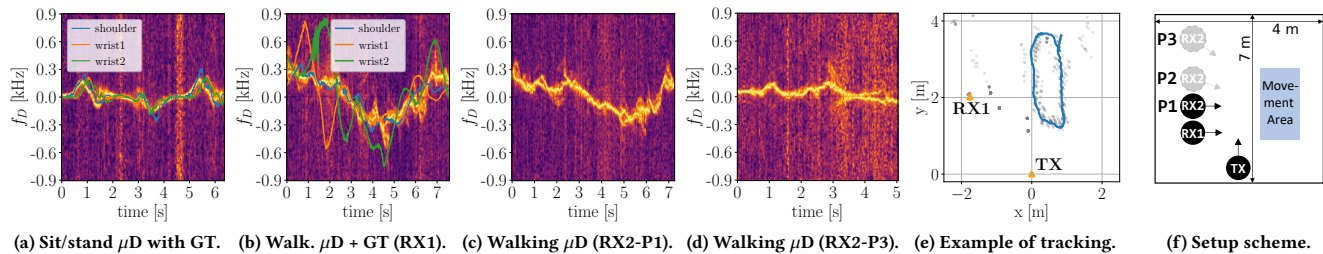


Figure 1: Experimental results and measurement setup scheme.

peaks in the CIR magnitude and select the first one, as the LoS always corresponds to the shortest path. After that, the CIR is shifted to make the LoS peak aligned with the first CIR tap. This operation is repeated for all time steps  $k$  and all BPs  $b$ .

**Target detection.** After this operation, to facilitate the detection of dynamic targets, static paths are removed from the CIRs. Since static paths are constant across time, we consider the time-averaged CIR, denoted as  $\tilde{h}_b(\ell)$ , to be a good estimate of the static background. Then, the foreground CIR amplitude is computed as  $\hat{h}_b(k, \ell) = \max(|h_b(k, \ell)| - \tilde{h}_b(\ell), 0)$ . At this point, dynamic target detections at time  $k$  are computed by applying a peak detection algorithm to  $\sum_{b=0}^{N_b-1} (\hat{h}_b(k, \ell))^2$ , being  $N_b$  the number of BPs. Finally, assuming the locations of TX and RXs are known, exploiting bistatic geometry [3] we compute the distance of the target from TX and the path's angle of departure, thus, localizing the target.

**Target tracking.** Based on the detected target locations, an Extended Kalman Filter (EKF) is built to track the movement of the targets, assuming they approximately follow a constant velocity model.

**CFO compensation and  $\mu$ D extraction.** To compute the  $\mu$ D spectrograms, we utilize multiple subsequent received packets. However, since the TX and RXs LOs are not precisely synchronized, every received packet is affected by a different CFO that spoils the  $\mu$ D reconstruction. Noting that every tap of a CIR have the same CFO, it is possible to isolate the CFO from a static path and use it to correct all paths. In our case, we use the LoS path as a reference to extract the CFO. Let  $\phi_{\text{off}}(k) = 2\pi f_{\text{off}}(kT)kT$  be the phase of the LoS path at time  $k$ . Then, the CFO-corrected CIR is given by  $\tilde{h}_b(k, \ell) = e^{-j\phi_{\text{off}}(k)} h_b(k, \ell)$ . After the correction, the resulting CIR can be used to compute the target's  $\mu$ D spectrogram as in [3].

### 3 EXPERIMENTAL RESULTS

**Implementation and Dataset.** The experimental setup is a customization of MIMORPH [2], based on the 60 GHz IEEE 802.11ay standard. It comprises 2 Xilinx Zynq UltraScale+ RFSoc ZCU111 boards (one for TX and one for RXs) and 3 Sivers EVK06002/00 antenna arrays with a radio frequency bandwidth of 1.76 GHz. TX and RXs are disposed according to 3 possible different setups, as shown in Fig. 1f. TX and RX1 are always positioned at the same locations, while RX2 is located at P1, P2, or P3, based on the setup. RXs point towards the movement area, to maximize the received signal-to-noise ratio of target's reflections. We acquired data from both RXs simultaneously. In total, we collected 72 sequences, 24 per setup, 36 per array. Within each setup, the subject performed two activities: walking along an oval trajectory or sitting down/standing up from a chair. Moreover, we acquired ground-truth data through

a marker-based motion capture system with millimeter level accuracy. Markers were placed on the antenna arrays and on some subject's body parts, namely: wrists, head, and shoulder. We use the head markers to precisely identify the location of the subject, the shoulder markers as an estimate of the chest movement, and the wrist markers as indicative of the arms movement.

**Results.** Fig. 1b-d show the  $\mu$ D obtained from the same walking activity when reflections are captured at different locations. We observe that the frequency of the Doppler shift decreases in P2 and P3. Since the bistatic angle  $\beta$  (the angle between TX and RX with vertex at the target) affects the Doppler frequency through a multiplicative factor  $\xi = \cos(\beta/2)$ , moving RX2 to P2 and P3 corresponds to approaching  $\beta = \pi$ , and, therefore,  $\xi$  decreases. Hence, our observation is in line with what expected from the theory. Fig. 1a-b show the  $\mu$ D reconstruction along with the estimate from the GT data. In Fig. 1a, with sit/stand activity, body parts undergo a similar movement and this is reflected in both  $\mu$ D and GT curves having the same shape. In Fig. 1b, the strongest  $\mu$ D component follows the movement of the chest, the largest body part, while the wrists movement align with the weaker components. Fig. 1e shows a sample tracking result, where in blue we show the EKF output.

### 4 CONCLUSIONS AND OUTLOOK

In this work, we presented the first experimental setup for *asynchronous and multistatic* ISAC in the mmWave frequency band. We collected a dataset featuring 1 TX and 2 RXs simultaneously receiving IEEE 802.11ay data packets. The dataset is supplemented with GT data that allows comparing, for the first time,  $\mu$ D traces with a quantitative and reliable reference. We show that LoS-based asynchrony resolution allows for accurate multistatic sensing without any kind of synchronization. This paves the way to new research to combine the information received at different nodes.

### REFERENCES

- [1] Zixiang Han, Lincong Han, Xiaozhou Zhang, Yajuan Wang, Liang Ma, Mengting Lou, Jing Jin, and Guangyi Liu. 2023. Multistatic Integrated Sensing and Communication System in Cellular Networks. *arXiv preprint arXiv:2305.12994* (2023).
- [2] Jesus O. Lacruz, Rafael Ruiz Ortiz, and Joerg Widmer. 2021. A Real-Time Experimentation Platform for Sub-6 GHz and Millimeter-Wave MIMO Systems (*MobiSys '21*). Association for Computing Machinery, New York, NY, USA, 427–439. <https://doi.org/10.1145/3458864.3466868>
- [3] Jacopo Pegoraro, Jesus O Lacruz, Tommy Azzino, Marco Mezzavilla, Michele Rossi, Joerg Widmer, and Sundeep Rangan. 2023. JUMP: Joint communication and sensing with Unsynchronized transceivers Made Practical. *arXiv preprint arXiv:2304.07766* (2023).
- [4] J Andrew Zhang, Kai Wu, Xiaojing Huang, Y Jay Guo, Daqing Zhang, and Robert W Heath. 2022. Integration of radar sensing into communications with asynchronous transceivers. *IEEE Communications Magazine* 60, 11 (2022), 106–112.